Rare Metal Materials and Engineering
Volume 52, Issue 12, December 2023
Available online at www.rmme.ac.cn

Science Press

Cite this article as: Zhang Jiarui, Yu Zhongdi, Wu Jinping. Effect of Recrystallization of Steel on Stability of Intermetallic Phases in Molten Al[J]. Rare Metal Materials and Engineering, 2023, 52(12): 4065-4072. DOI: 10.12442/j.issn.1002-185X.20230258.

ARTICLE

Effect of Recrystallization of Steel on Stability of Intermetallic Phases in Molten Al

Zhang Jiarui[1], Yu Zhongdi[2], Wu Jinping[2]

[1] School of Materials Science and Engineering, Northeastern University, Shenyang 110819, China; [2] Xi'an Rare Metal Materials Institute Co., Ltd, Xi'an 710016, China

Abstract: The influence of steel's recrystallization on the stability of intermetallic compounds (IMCS) layer was investigated in molten Al at 700 °C. Results show that high degree of structural rearrangement leads to the formation of non-protective IMCS layer on the 304SS surface and its corrosion kinetics coincides with linear law. Compact and stable Fe_2Al_5 layer delays the failure of the 410SS in liquid Al. The stability of IMCS is affected by steel's recrystallization in three aspects: (1) energy for IMCS nucleation and growth are reduced, especially for Fe_4Al_{13}; (2) grain orientation transforms to close-packed direction which slows down the diffusion rate of Al ion; (3) stress mismatch is increased at the IMCS/steel interface, especially for the austenitic 304SS.

Key words: stainless steel; recrystallization; molten Al corrosion

Hot-dipping aluminum is an economic method for boilers and exhaust steel pipes protection in high-temperature environment[1–3]. By forming continuous alumina layer, oxidation of the matrix is prevented. However, thick intermetallic compounds (IMCS) formed at Al/steel interface threaten the stability of the coating, especially under thermal shock case. Quite different thermal expansion of the IMCS and steel increases interfacial stress concentration, promoting microcracks initiation within this layer[4–6]. As the reaction of steel with liquid-Al is thermodynamically spontaneous, the research on aluminized steel degradation by IMCS formation is meaningful to guide its production [7].

Over the last decades, the evolution of IMCS on aluminized mild steel has been researched widely. Double-layer structure of the inner tongue-like Fe_2Al_5 (η phase) and outer flocculent Fe_4Al_{13} (θ phase) are observed in ferrite steel after dipping in molten Al[8–11]. The growth of this layer is affected by outer θ phase dissolution and element interdiffusion in the inner η phase. This model is suitable for most low-alloying steels with bcc structure, while some abnormal results are reported for the austenitic or martensitic steel in recent years[12–15]. Chen et al[16] studied the effect of austenitic process on the ST12 steel in liquid aluminum. After austenitizing treatment, tongue-like Fe_2Al_5/α-Fe transforms to flat Fe_2Al_5/γ-Fe interface. Similarly, Li et al[17] observed a flat IMCS layer on the austenitic SAE201 stainless steel surface, which is different from the rough products on the mild steel. Obviously, microstructure difference of steel will significantly affect the structure of IMCS layer.

In recent years, a lot of stainless steels have been used for aluminized plating to meet growing high-temperature serving demands. However, inevitable recrystallization occurs in austenitic or martensitic steel during hot-dipping process[18–19]. This matrix structural transition can release the stored energy generated in the deformation process, affecting interfacial Fe-Al phase nucleation and growth. Since few of researches report this structural rearrangement issue, it is urgent to clarify the influence of recrystallization on interfacial IMCS layer formation.

In this study, two commercial stainless steels were researched, including martensitic 410SS and austenitic 304SS. These commercial stainless steels are widely used in corrosive and high temperature environment. To simulate hot-dipping condition, these steels were immerged in pure aluminum at 700 °C. This temperature is high enough for these steels to recrystallize. The evolution of interfacial Fe-Al phase was

Received date: May 01, 2023
Foundation item: Natural Science Foundation of Shaanxi Province (2022JQ-452); Qinchuangyuan Project of Shaanxi Province (QCYRCXM-2022-189); RMMI Research Project (K2206S)
Corresponding author: Yu Zhongdi, Ph. D., Xi'an Rare Metal Materials Institute Co., Ltd, Xi'an 710016, P. R. China, E-mail: yzdneu2018@163.com

also researched.

1 Experiment

1.1 Annealing experiment

The composition of austenitic stainless steel (304SS) and martensitic stainless steel (410SS) is shown in Table 1. All the annealed samples were prepared with the dimensions of 12 mm×10 mm×2 mm. In order to reveal the structure evolution, these samples were heated to 700 °C for 3, 5, 10, 30 and 60 min, and then air cooled.

1.2 Dipping experiment

For hot-dipping Al test, steel samples were polished with 800# metallographic sandpaper to remove surface impurities and oxides. Then, original size and mass of samples were measured.

During each test, 50 g industrial pure aluminum (99.9%) and five parallel samples were set in corundum crucible. Then, they were heated to 700 ° C in high temperature furnace. After test, these dipped samples were taken out and air cooled.

1.3 Characterization

In order to calculate the mass change of these samples, dipped samples were immersed in 20wt% NaOH solution to remove adhered aluminum. Then, they were cleaned, dried and weighed. These samples for cross-sectional observation were polished with adhered Al.

The Rockwell hardness tester and optical microscope were used to measure the hardness and macrostructure evolution after annealing. Scanning electron microscope (SEM) was used to observe the micromorphology of the corrosion products. X-ray diffraction analysis (XRD) was used for phase identification. Microhardness and Young's elastic modulus of the IMCS layer and matrix were researched by nanoindentation technology. The EBSD technique was taken to detect the grain orientation of the alloy matrix.

2 Results and Discussion

2.1 Recrystallization texture

Fig. 1 shows the microhardness and microstructure of the 304SS and 410SS after annealing at 700 °C for different time. After heat treatment for 60 min, the microhardness of the 304SS reduces sharply from 228×9.8 MPa to 180×9.8 MPa, especially at the initial 10 min. This change also matches with its microstructure evolution, i. e. these elongated grains have transformed to equiaxed crystals after annealing for 10 min. For the 410SS, its microhardness gradual decreases from initial 168×9.8 MPa to 140×9.8 MPa. Various equiaxed crystals grow slightly in this steel. Obviously, recrystallization occurs in these steels, especially the 304SS.

Table1 Composition of 304SS and 410SS samples (wt%)

Sample	Fe	Cr	Ni	Mn
304SS	72	18	8	2
410SS	86.5	13	0	0.5

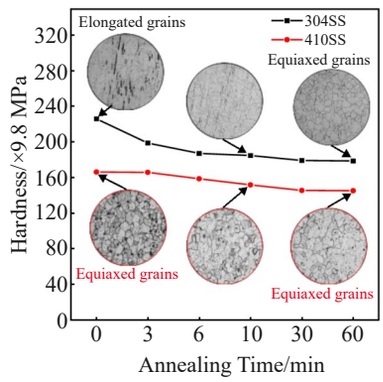

Fig.1 Tempering transformation of microhardness and microstructure of 304SS and 410SS

2.2 Corrosion kinetics and phases

Fig. 2 shows the corrosion kinetics of the 304SS and 410SS samples in liquid aluminum at 700 °C. For the 304SS, its mass change curve fits with linear laws roughly. After corrosion for 60 min, its mass loss reaches to 0.48 mg/mm^2. Much lower corrosion rate is observed for the 410SS and an obvious incubation period occurs at the initial period. Thereafter, its corrosion rate increases gradually. Different corrosion kinetics is related with their recrystallization behavior. Referring to their kinetics, these samples are researched at three periods: 3, 10 and 60 min.

Fig. 3 shows the XRD results of IMCS on the 304SS and 410SS after corrosion for different time. Both of Fe_2Al_5 and Fe_4Al_{13} phases are detected on these two steels but in different ratios. For the 304SS, strong diffraction peaks of Fe_2Al_5 and Fe_4Al_{13} phases are detected just after 3 min. Thereafter, most Fe_4Al_{13} peaks are missing, leaving Fe_2Al_5 as the main phase after 60 min corrosion. For the 410SS, Fe_2Al_5 is the major product during the whole test, and weak peak of the Fe_4Al_{13}

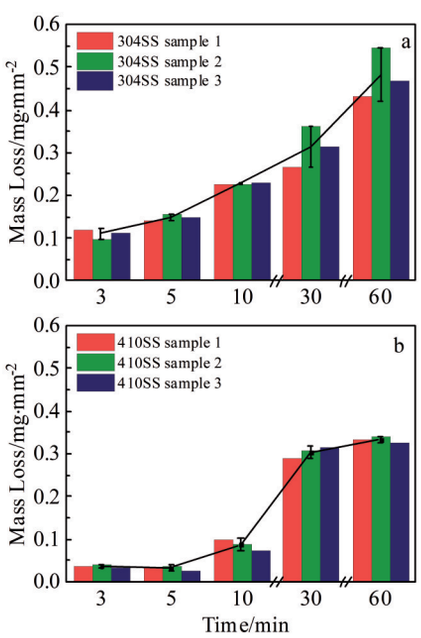

Fig.2 Corrosion kinetics curves of 304SS (a) and 410SS samples (b)

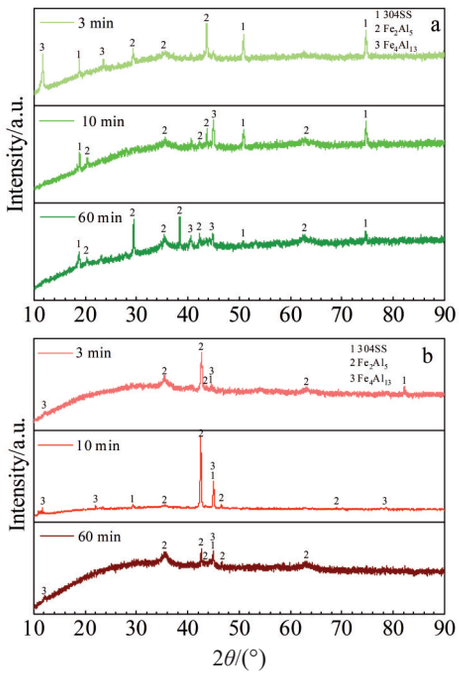

Fig.3 XRD patterns of 304SS (a) and 410SS (b) after corrosion in molten aluminum at 700 °C for different time

phase even cannot be detected. Obviously, recrystallization accounts for different Fe_4Al_{13}/Fe_2Al_5 ratios on these steels.

2.3 Intermetallic compounds structure

In order to clarify the effect of recrystallization on IMCS growth, their microstructure, elements distribution and mechanical properties were researched in detail.

The microstructures of the IMCS on the 304SS are shown in Fig. 4. After immerging in liquid-Al for 3 min, the 304SS surface turns to loose and porous. Spongy and acicular phases completely cover its surface (Fig. 4a). Thereafter, many large-size holes are observed on this IMCS surface, as shown in Fig. 4b. These deep holes provide rapid diffusion channels for liquid Al to erode the matrix continuously. Then, loose IMCS layer spalls off the 304SS easily, leading to its pitting (Fig. 4c).

Different from the case of the 304SS, much flatter IMCS surface morphology is observed on the 410SS, as shown in Fig. 5. Uniformly distributed rod-like phases cover the 410SS surface just after 3 min test. Extending corrosion to 10 min, the morphology of IMCS shows no obvious change. Only some microcracks are initiated on surface, as shown in Fig. 5b. The crack density on the IMCS further increases after 60 min corrosion, while no deep corrosion hole is found, as shown in Fig. 5c.

The cross-sectional microstructure of the IMCS on the 304SS is shown in Fig. 6. At the initial stage, an IMCS layer with loose outer sublayer and dense inner sublayer is observed on this steel (Fig. 6a). Referring to XRD patterns and other researches[8–11], the IMCS layer consists of outer Fe_4Al_{13} and inner Fe_2Al_5. This IMCS layer is unstable and many island-like Fe_4Al_{13} phases peel off its surface just after 3 min corrosion. Various microcracks are initiated in the porous Fe_4Al_{13} layer, accelerating its detachment. Then, quite a lot of flocculent phases are observed on the IMCS surface (Fig. 6b). Since this interfacial layer fails to prevent element interdiffusion, the outer Fe_4Al_{13} layer breaks down after corrosion for 60 min. Significant recrystallization of this steel accounts for unprotective products and linear kinetic curve of the 304SS (Fig.2).

Much thicker IMCS layer is observed on the 410SS surface in Fig. 7. The dense Fe_2Al_5 layer, about 25 μm in thickness, shows typical tongue-like characteristics. This rough interface is in favor of the IMCS stability and it maintains the same thickness during initial 10 min (Fig. 7b). This phenomenon

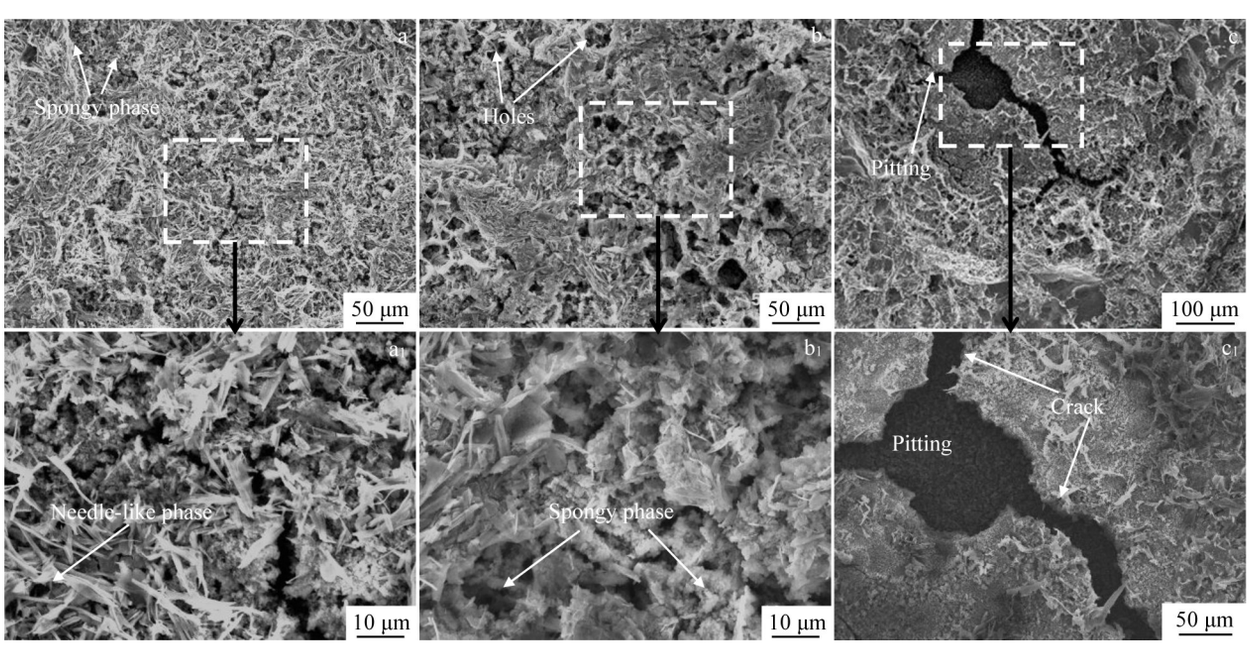

Fig.4 Microstructures of the IMCS on 304SS after corrosion for different time: (a, a_1) 3 min, (b, b_1) 10 min, and (c, c_1) 60 min

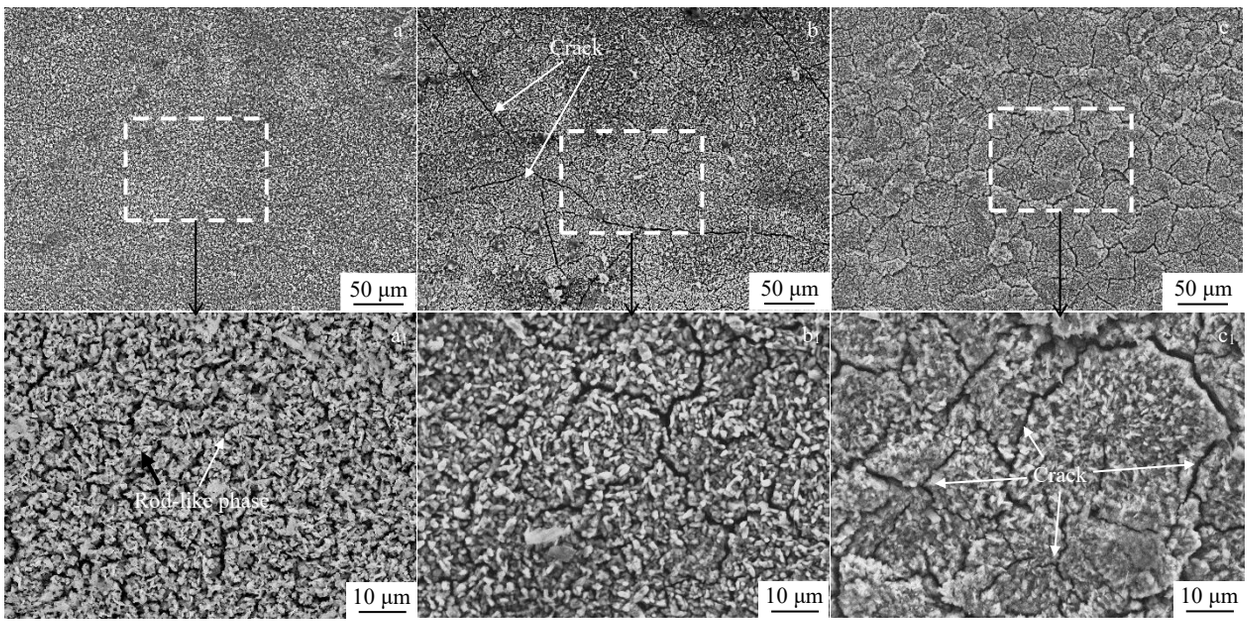

Fig.5 IMCS surface morphologies on 410SS after corrosion for different time: (a, a_1) 3 min, (b, b_1) 10 min, and (c, c_1) 60 min

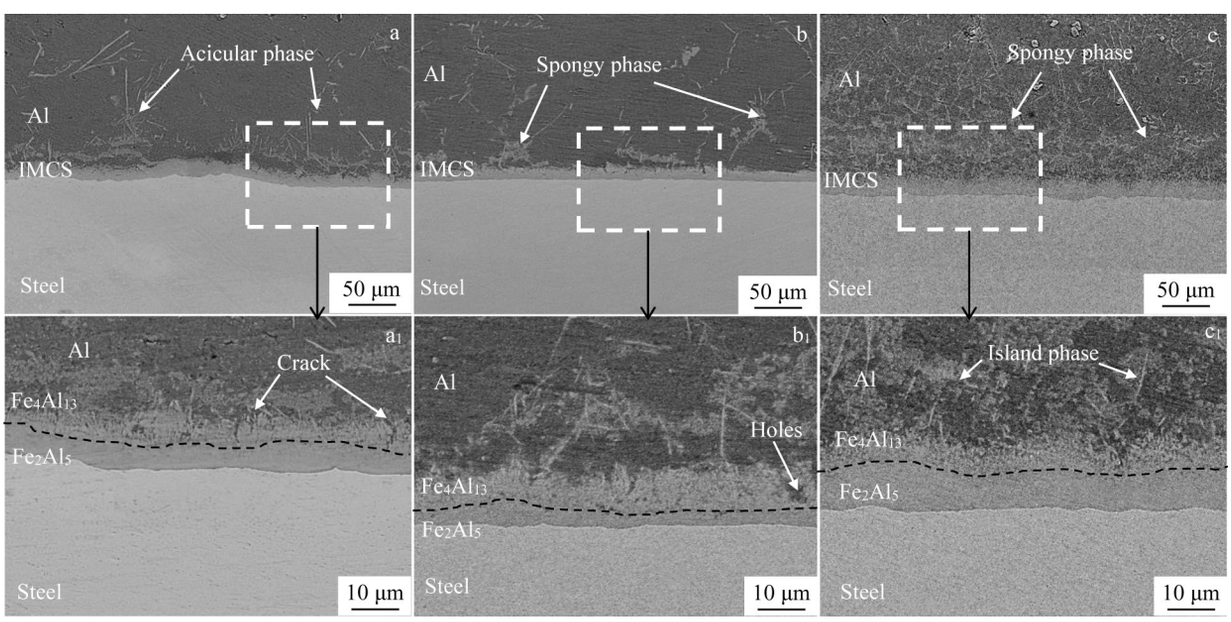

Fig.6 Cross-sectional microstructures of the IMCS on 304SS after corrosion for different time: (a, a_1) 3 min, (b, b_1) 10 min, and (c, c_1) 60 min

also explains its incubation period in kinetics. Further extending corrosion to 60 min, the IMCS layer still keeps compact. Quite a few Fe_4Al_{13} particles dissolve into liquid-Al as shown in Fig. 7c. The high stability of this layer is also related with slight substrate recrystallization.

In order to clarify the difference of IMCS on these two steels, its EDS elemental line scanning was used. As the product on the 304SS begins to degenerate after 10 min dipping test, elemental distribution on these two steels was analyzed at this case. These alloying elements in two stainless steels gradually dissolve into the melt. But quite different distribution tendency of Al is detected along the Fe-Al layer on these steels in Fig. 8. For the 304SS, the content of Al changes sharply at the Fe_4Al_{13}/Al and Fe_2Al_5/substrate interfaces. However, the content of Al increases gradually from the matrix to Al side on the 410SS. Different element transformation mechanisms in Fe-Al layer accounts for elemental distribution discrepancy.

Nanoindentation curves of the steel matrix and IMCS layer after 10 min corrosion are shown in Fig. 9[20]. The peak load (green curve) of 304SS is higher than that of 410SS, matching with the Rockwell hardness result. The harder 304SS shows lower modulus than the 410SS in Table 2. For the IMCS layer, both of the hardness and modulus (red curve) of the 304SS are lower than those of 410SS. Referring to Ref.[21–22], the ratio of H/E also can be used to evaluate the IMCS layer's tough-

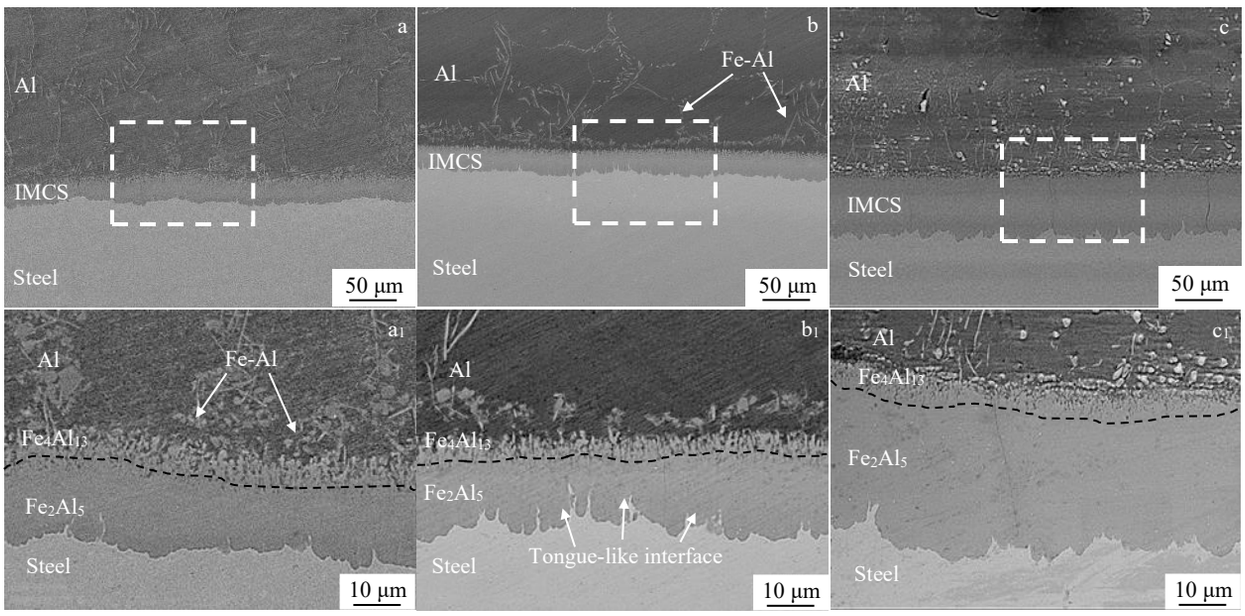

Fig.7 Cross-sectional microstructures of 410SS after corrosion for different time: (a, a_1) 3 min, (b, b_1) 10 min, and (c, c_1) 60 min

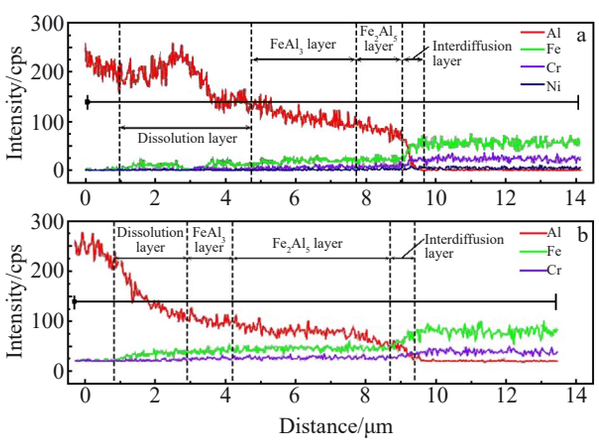

Fig.8 EDS elemental distribution of compound layer on 304SS (a) and 410SS (b) after 10 min corrosion

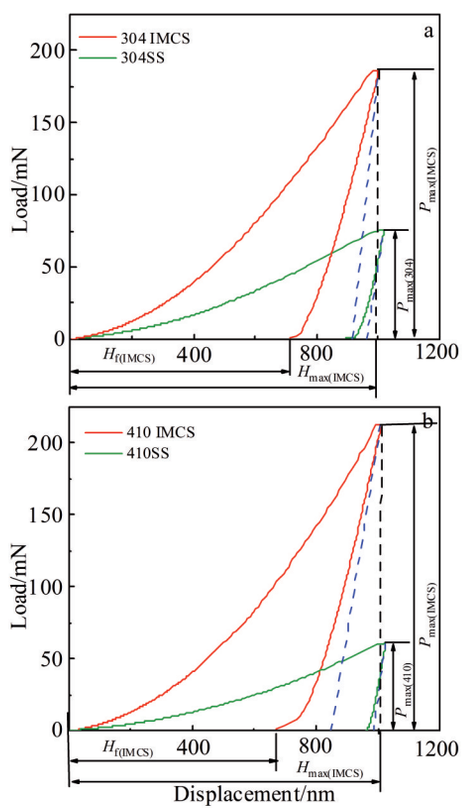

Fig.9 Nanoindentation load-displacement curves of compound layer and matrix on 304SS (a) and 410SS (b) after corrosion for 10 min

ness. For the 304SS, this value (0.047) is lower than that of 410SS (0.050), indicating the better toughness of the IMCS on the later alloy. This result also matches with the high spallation tendency of Fe-Al layer from the 304SS matrix.

Above results reveal that recrystallization of these steels indeed affects the stability of IMCS layer in liquid Al. In order to illustrate the influence of this grain orientation rearrangement, the subsurface microstructures of two steels were analyzed by EBSD after 10 min corrosion. As shown in Fig. 10, strong (001) oriented structure is observed in the RD of the 304SS, matching with the silk texture observed in Fig. 1. Along the ND, (111) and other oriented structure are detected. For the 410SS, strong (001) and (111) oriented structures are observed in the TD and ND, respectively. As the major corrosion of steel plate sample is along ND, the grain orientation in this direction will affect its corrosion behavior significantly.

For the 304SS, recrystallization happens at 700 °C. This structure transformation accelerates the degeneration of porous IMCS on this steel, leading to its linear corrosion kinetics. For the 410SS, slight corrosion occurs in this alloy due to its high structure stability. Dense interfacial Fe_2Al_5 layer formed on this steel delays the substrate dissolution. In

Table 2 Mechanical properties of IMCS layer and matrix

Sample	Hardness/GPa	Modulus/GPa
304SS	3.7	205.1
304SS IMCS	8.53	179.7
410SS	2.92	216.6
410SS IMCS	9.79	194.4

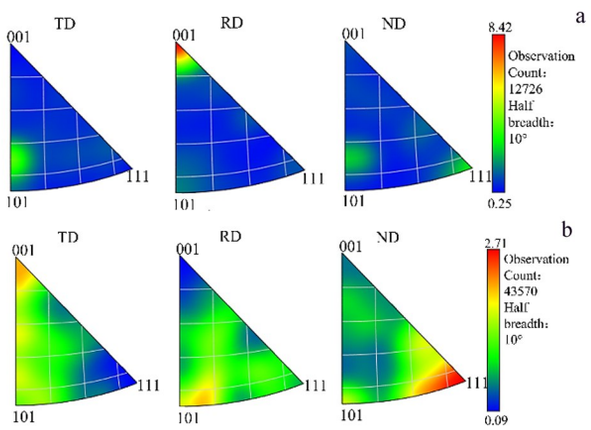

Fig.10 Reverse pole diagrams of matrix 304SS (a) and 410SS (b) grain orientation after corrosion for 10 min

the following part, the effect of steel recrystallization on the evolution of IMCS is discussed from corrosion dynamics, thermodynamics and microstructure.

2.4 Corrosion dynamics

Different corrosion dynamics is observed for the 304SS and 410SS after dipping in molten Al for 60 min. The kinetic curve of the 304SS follows linear laws, while an obvious incubation period is observed on the 410SS. During hot-dipping in liquid-Al, the total mass change of the matrix Δ_M is determined by the amount of inward diffusion of Al atoms Δ_{Al} and outward dissolution of Fe atoms Δ_{Fe}, as shown in Fig.11[23–24].

$$\Delta_m = \Delta_{Al} + \Delta_{Fe} \quad (1)$$

As shown in Fig. 11, when $\Delta_{Al} > \Delta_{Fe}$, the growth of Fe_2Al_5 layer toward steel substrate is faster than that of Fe_4Al_{13} layer dissolving into liquid aluminum. Then, the IMCS layer becomes thicker. When $\Delta_{Al} < \Delta_{Fe}$, the thinner IMCS layer is related to the fast dissolution of Fe_4Al_{13} layer. Under the case of $\Delta_{Al} = \Delta_{Fe}$, the thickness of IMCS layer remains stable. This difference of IMCS thickness is related with their mass transportation discrepancy, caused by different recrystallization behavior.

In this study, the thickness of IMCS layer on the 304SS roughly remains a constant, matching $\Delta_{Al} = \Delta_{Fe}$ condition. Loose Fe-Al phase cannot prevent the outward dissolution of alloying elements. A great amount of holes and cracks in the Fe_4Al_{13} layer provide preferential channels for the rapid diffusion of Al, as shown in Fig. 4 and Fig. 6. Moreover, significant variation of Al is observed at substrate/IMCS interface in Fig. 8. This result reveals that element dissolution rate through these defects determines its corrosion.

For the 410SS, the IMCS layer becomes thicker after 10 min,

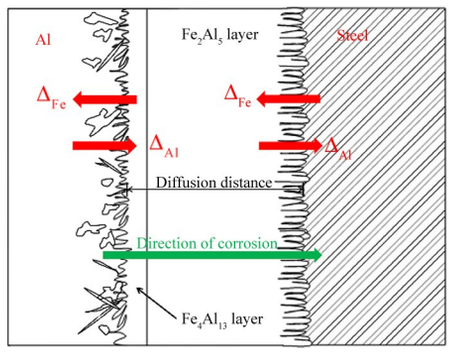

Fig.11 Fe/IMCS/Al interface diffusion diagram

confirming $\Delta_{Al} > \Delta_{Fe}$ within this steel. Elemental interdiffusion guides the growth of IMCS layer on this steel, as confirmed by an incubation period in its kinetic curve (in Fig. 2). Under the protection of thick and dense IMCS layer, preferential diffusion of Al through the *c*-axis of Fe_2Al_5 lattice accounts for its tongue-like interfacial structure in Fig. 7. This mass transportation pattern delays the failure of the 410SS[25–27].

Different recrystallization degree accounts for the diversity of Δ_{Al}/Δ_{Fe} on these steels. Deformation stress is released during this structural rearrangement, accompanied with matrix softening. The microhardness of the 304SS has decreased by 20.7% after 60 min annealing, while this decrement is 13.7% for the 410SS. Such high recrystallization degree of the 304SS increases its stress concentration at the IMCS/steel interface. Due to the poor deformation capacity of the intermetallic Fe-Al layer, various cracks are initiated at the IMCS/304SS interface, as shown in Fig. 6. These defects build up fast channels for mass transformation through the IMCS layer and the amount of Δ_{Al} is equal to Δ_{Fe} on the 304SS. On the contrary, the lower stress concentration ensures the stability of IMCS on the 410SS. The growth of IMCS is guided by the lower Δ_{Fe} on this steel.

2.5 Corrosion thermodynamics

For these two stainless steels, two Fe-Al phases are detected during test. In thermodynamics, the Gibbs free energy for the Fe_2Al_5 and Fe_4Al_{13} formation at 973 K is calculated as follows[7, 28].

$$2Al + 5Fe = Fe_2Al_5,\ \Delta G = -19.6\ \text{kJ/mol} \quad (2)$$

$$13Al + 4Fe = Fe_4Al_{13},\ \Delta G = -22.9\ \text{kJ/mol} \quad (3)$$

Similar reaction energy of Eq. (2) and Eq. (3) indicates that the two reactions occur spontaneously during this test. However, different ratios of Fe_2Al_5/Fe_4Al_{13} are observed for these two steels. This discrepancy is related with their recrystallization degree, which can offer stored deformation energy for reactions. For the 304SS, its original strip structure gradually transforms to equiaxed-grain just after annealing at 700 °C for 10 min, as shown in Fig.1. Released stain energy is in favor of Fe-Al phase nucleating on this steel surface, especially for the Fe_4Al_{13}. That is, the thickness of Fe_4Al_{13} layer is about 1.5 times larger than that of the Fe_2Al_5 on the 304SS. This phenomenon is quite different from much thinner Fe_4Al_{13} layer observed on the 410SS, which suffers slight

recrystallization. So the formation of Fe_4Al_{13} on steel is closely related with this matrix structural rearrangement.

2.6 Surface texture

Different surface textures are detected on the two stainless steels after their recrystallization. As the ND is parallel to diffusion path of Al ion, the orientation of matrix structure along ND affects steel's corrosion significantly. In Fig.10, the two steels display the preferred [111] orientation along the ND.

For the austenite 304SS, [111] direction is perpendicular to (111) plane, which is the close-packed plane in fcc structure. The crystal face spacing of the (111) plane (0.2073 nm) is an order of magnitude larger than the gap of two adjacent iron atoms on this plane (about 0.02 nm). So aluminum atoms (radius=0.163 nm) tend to enter into the gap of two close-packed (111) planes of the 304SS. This result also explains loose Fe_4Al_{13} layer and its lamellar detachment in Fig.6.

For the martensitic 410SS, its matrix phase transforms to sorbite (bcc structure) during annealing, as shown in Fig. 1. The [111] orientation is the close-packed direction in bcc structure. Along this direction, the crystal face spacing of (111) is 0.1666 nm, which is close to aluminum atom radius (0.163 nm). It is difficult for Al ion to enter into the gap of (111) face on the 410SS after recrystallization.

Apart for the influence on Al ion diffusion, surface texture also causes different degrees of stress concentration at IMCS/steel interface[29–30]. This stress mismatch (C_e) can be calculated by the following formula:

$$C_e = E_{IMCS}/E_{Fe} \quad (4)$$

where E_{IMCS} is the IMCS layer modulus, E_{Fe} is the matrix modulus. Taking the data in Table 2, $C_e \approx 0.876$ for 304SS, and $C_e \approx 0.897$ for 410SS. It can be concluded that the modulus matching of 304SS is worse than that of 410SS. When the 304SS suffers thermal shock, the higher internal stress at IMCS/steel interface will weaken its boundary.

3 Conclusions

1) Loose and non-protective intermetallic compounds layer on the 304SS leads to linear corrosion kinetics, while thick and dense layer on the 410SS delays its failure.

2) Notable recrystallization on the 304SS reduces the energy for Fe-Al phases nucleation and growth, especially for Fe_4Al_{13}.

3) Slight structural rearrangement of the 410SS along its close-packed direction prevents the fast diffusion of Al.

4) Matchable stress of the Fe-Al layer and matrix is in favor of its well-adhesion.

References

1 Frutos E, Álvarez D, Fernandez L *et al*. *Journal of Alloys and Compounds*[J], 2014, 617: 646

2 Lemmens B, Springer H, Peeters M *et al. Materials Science and Engineering A*[J], 2021,710: 385

3 Chen G, Xue L, Wang J *et al. Corrosion Science*[J], 2020, 174: 108 836

4 Xu G, Wang K, Dong X *et al. Journal of Materials Science and Technology*[J], 2021,71: 12

5 Shi L, Kang J, Qian C *et al. Materials Science and Engineering A*[J], 2022, 831: 142 233

6 Deng Z, Xiao H, Yu C. *Materials Design*[J], 2022, 222: 111 106

7 Prasanthi T N, Sudha C, Rebby P. *Surface and Coatings Technology*[J], 2022, 440: 128 456

8 Takata N, Nishimoto M, Kobayashi S *et al. Intermetallics*[J], 2015, 67: 1

9 Cheng W, Wang C. *Surface and Coatings Technology*[J], 2009, 204: 824

10 Luo Q, Liu W, Li W *et al. Journal of Materials Research and Technology*[J], 2022, 17: 452

11 Awan G H, Hasan F. *Materials Science and Engineering A*[J], 2008, 472: 157

12 Dangi B, Brown T W, Kulkarni K N. *Journal of Alloys and Compounds*[J], 2018, 769: 777

13 Huilgol P, Udupa K, Bhat K U. *Surface and Coatings Technology*[J], 2018, 348: 22

14 Liu B, Yang Q, Wang Y. *Results in Physics*[J], 2019, 12: 514

15 Cheng W J, Wang C J. *Applied Surface Science*[J], 2013, 277: 139

16 Chen S, Yang D, Zhang M *et al. Metallurgical and Materials Transactions A*[J], 2016, 47: 5089

17 Li Y, Jia Q, Zhu Z *et al. Surface Review and Letters*[J], 2017, 24: 1 750 046

18 Derazkola H A, Garcia E, Marrodán A M *et al. Journal of Materials Research and Technology*[J], 2022, 18: 2293

19 Huang K, Logé R. *Materials Design*[J], 2016, 111: 548

20 Oliver W, Pharr G. *Journal of Materials Research*[J], 1992, 7: 1564

21 Chen X, Du Y, Chung Y. *Thin Solid Films*[J], 2019, 688: 137 265

22 Musil J, Kunc F, Zeman H *et al. Surface and Coatings Technology*[J], 2002, 154: 304

23 Zhang J, Hosemann P, Maloy S. *Journal of Nuclear Materials*[J], 2010, 404: 82

24 Dybkov V. *Journal of Materials Science*[J], 1990, 25: 3615

25 Azimaee H, Sarfaraz M, Mirjalili M *et al. Surface and Coatings Technology*[J], 2019, 357: 483

26 Jeshvaghani R, Emami M, Shafiee O *et al. Surface and Coatings Technology*[J], 2014, 240: 365

27 Cheng W J, Wang C J. *Applied Surface Science*[J], 2013, 277: 139

28 Rong J, Kang Z, Chen S *et al. Materials Characterization*[J], 2017, 132: 413

29 Patra L, Pandey R. *Materials Today Communications*[J], 2022, 31: 103 626

30 Surya R, Siddhartha P. *Acta Materialia*[J], 2008, 56: 3523

再结晶对钢在铝液中形成的界面相稳定性影响

张佳锐[1]，余中狄[2]，吴金平[2]
(1. 东北大学 材料科学与工程学院，辽宁 沈阳 110819)
(2. 西安稀有金属材料研究院有限公司，陕西 西安 710016)

摘　要：研究了钢的再结晶对热浸铝过程金属间化合物（IMCS）层的稳定性影响，结果表明：304不锈钢在热浸镀过程的再结晶结构重排造成该钢材表面形成了非保护性IMCS层，该合金的腐蚀动力学满足线性规律；再结晶程度较轻的410不锈钢表面形成了稳定且致密的Fe_2Al_5层，该层延缓了其在热浸铝过程的失效。钢材的再结晶对于热浸镀铝过程中界面金属间化合物的影响包括：（1）再结晶可降低IMCS的形核和生长能量，尤其是Fe_4Al_{13}相；（2）再结晶引起的晶粒沿密排方向排布可降低Al离子的扩散速率；（3）再结晶加剧了IMCS/钢界面处的应力失配，尤其是奥氏体钢。

关键词：不锈钢；再结晶；液态铝腐蚀

作者简介：张佳锐，男，1999年生，硕士，东北大学材料与工程学院，辽宁 沈阳 110819，E-mail：2170580@stu.neu.edu.cn